ARTICLE   OPEN

Check for updates

Non-planar graphene directly synthesized on intracavity optical microresonators for GHz repetition rate mode-locked lasers

Oleksiy Kovalchuk[1,2,5], Sungjae Lee[1,2,5], Hyowon Moon[1,2], Andrea M. Armani [ID][3,4,✉] and Yong-Won Song [ID][1,2,✉]

Generation of high-speed laser pulses is essential for sustaining today's global, hyper-connected society. One approach for achieving high spectral and temporal purity is to combine optical nonlinear materials with spectral filtering devices. In this work, a graphene-coated microresonator integrates a nonlinear material and a spectral filtering platform into a single device, creating a tunable GHz repetition rate mode-locked fiber laser. The graphene is directly synthesized on the non-planar surface of microresonator, resulting in a uniform, conformal coating with minimal optical loss in the device. The whispering gallery modes of the resonator filter the propagating modes, and the remaining modes from the interaction with graphene lock their relative phases to form short pulses at an elevated repetition rate relying on inter-modal spectral distance. Additionally, by leveraging the photo-thermal effect, all-optical tuning of the repetition rate is demonstrated. With optimized device parameters, repetition rates of 150 GHz and tuning of 6.1 GHz are achieved.

INTRODUCTION

The global community has acknowledged that there are increasing societal demands for high-capacity data management, processing, and transmission. One potential solution is improving data transfer by leveraging passive ultra-short laser pulse generation[1,2]. In particular, its high pulse repetition rate defines the data transfer and sampling rates, spectrum density, and energy distribution[3–5]. Given that needs for data management span from particle physics research to securing global communications networks, developing more energy efficient data transfer methods will have broad societal impact[6,7].

Conventional approaches for creating ultra-high repetition rate lasers include high-speed external modulation, high harmonic generation, and cavity length customization[8–10]. One elegant strategy integrates additional intracavity components that provide spectral filtering to control the transform-limited laser pulses generated by pulse-forming devices or nonlinear optical materials. In previous works, optical resonant cavity-based filters have been combined with saturable absorbers to successfully achieve ultra-high repetition rate lasers[11–17].

In this context, one exciting saturable absorber is graphene. With an exceptional third-order nonlinear coefficient ($\chi^{(3)} \sim 10^{-19}$ $m^2\,V^{-2}$) and a wide operation spectral window[18–20], graphene has generated passively mode-locked laser pulses with femtosecond durations[21–23]. Its ultra-fast carrier mobility and low saturation threshold energy ensure ultra-short but highly stable output laser pulses. To further push the performance and increase the speed, graphene layers have been combined with optical resonant devices previously[24–28]. In spite of these achievements, the reported works (Supplementary Table 1) in the GHz-repetition rate regimes relied on a graphene transfer process that resulted in limited area and non-uniform graphene coverage on the photonic

device, fundamentally limiting performance[24,25,27]. Therefore, to overcome these barriers requires re-imagining the resonant cavity structure and cavity material as well as the graphene deposition approach.

One possible solution is found by combining high quality factor (Q) silica whispering gallery mode (WGM) optical resonant cavities with the atomic carbon spraying (ACS) method for graphene deposition[28,29]. Briefly, the silica resonator serves as an optical filter with the cavity free spectral range (FSR) determining the pulse train frequency. The graphene layer behaves as a saturable absorber and further purifies the spectrum by removing modes with weak intensities. Given this mechanism, both the material purity and deposition uniformity of the graphene and the device performance must be maintained in order to realize the GHz repetition rate mode-locked fiber laser which provides further reconfigurability, tunability, and versatility for conventional laser systems.

In the present work, we overcome both the material and device hurdles to demonstrate a GHz repetition rate mode-locked fiber laser. To minimize the loss of the coating, graphene is directly synthesized on the microsphere resonant cavity surface. The ACS method enabled a conformal and uniform layer to be achieved on the non-planar cavity surface. The microsphere can be an attractive option in future integrated optical platforms due to its high fabrication process efficiency as long as the nonlinear interaction of the WGM with the graphene layer is verified[29]. This graphene-coated microcavity serves as a passively controlled intracavity component in the system, and repetition rates as high as 150 GHz are achieved. Additionally, by coupling a secondary control laser into the main cavity, the photo-thermal effect of graphene enables tuning of the pulse repetition rate up to 6.1 GHz.

[1]Center for Opto-Electronic Materials and Devices, Korea Institute of Science and Technology, Seoul 02792, Republic of Korea. [2]Nanoscience and Technology, University of Science and Technology, Daejeon 34113, Republic of Korea. [3]Mork Family Department of Chemical Engineering and Materials Science, University of Southern California, Los Angeles, CA 90089, USA. [4]Ellison Institute of Technology, Los Angeles, CA 90064, USA. [5]These authors contributed equally: Oleksiy Kovalchuk, Sungjae Lee. [✉]email: armani@usc.edu; ysong@kist.re.kr
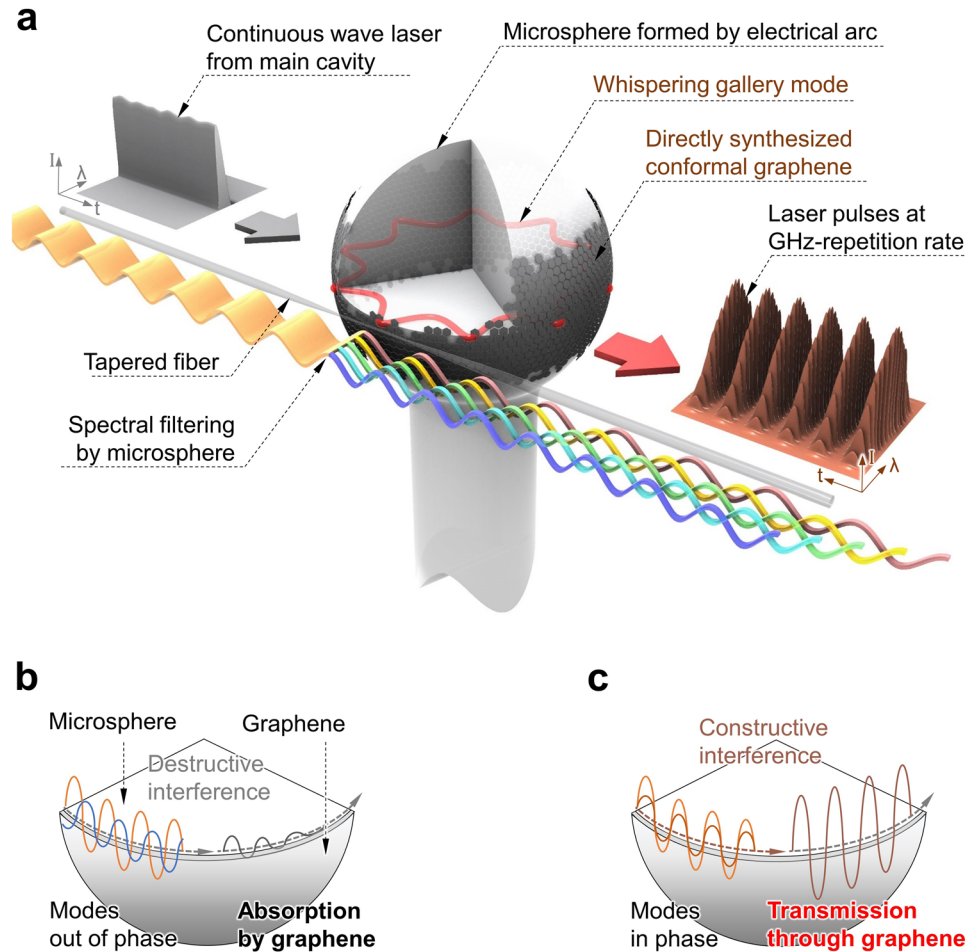
Fig. 1 Illustration of the operating principle. a Due to the long photon lifetime inside of the cavity and the narrow resonant linewidth, the optical field is intrinsically amplified, and the input spectrum is filtered. As a result of the interaction between the high intensity optical fields and the graphene coating, laser pulses are formed at GHz repetition rates. Colored waves represent the modes that remain after the graphene phase-locked with each other to form the short pulses displaying temporally periodic constructive interferences at GHz repetition level. **b** Destructive interference between WGMs with random phases and absorption by conformal graphene on microsphere surface. **c** WGMs with locked phases constructively interfere and transmit through graphene.

RESULTS AND DISCUSSION

### Generation of ultra-short pulse with ultra-high repetition rate

Figure 1a provides an overview of the generation mechanism of the GHz pulsed laser based on a graphene-coated resonant microcavity. The designed device is inserted into a fiber ring laser cavity and acts as a passively operating mode-controller. As shown in Fig. 1, there are three processes that contribute to the pulse formation sequence. First, the primary continuous wave (CW) laser is formed inside the main laser cavity as a function of gain, loss, and state of polarization. Second, the CW laser signal is spectrally filtered by the resonances of the high-Q optical microcavity. The resonant wavelengths are determined by the microsphere diameter and effective refractive index[30]. Third, the graphene layer assists in the mode-locking of selected optical modes to form an ultra-short pulse. The specific mechanism of pulse formation is notable and can be explained by the Pauli-blocking principle (Fig. 1b, c)[22,31]. The repetition rate is governed by the FSR of the cavity or the spacing between adjacent optical modes. Based on this combination of mechanisms, it is clear why achieving both a high-Q device and a loss-minimized graphene layer will support the generation of a wider spectral envelope, thereby guaranteeing a larger number of filtered modes with shorter pulse duration.

Fabrication and characteristics of microspheres

The fabrication of the graphene-coated microsphere resonators combines two processes: fabrication of silica high-Q resonant cavities and conformal synthesis of uniform graphene layer.

Conventional silica microsphere cavities are based on a thermally-induced reflow[32–34]. In this work, an arc fusion approach is developed. By controlling the arc parameters and the initial fiber diameter, it is possible to achieve a wide range of sphere sizes (Fig. 2a). A detailed fabrication process is described in supplementary information. Atomic force microscopy (AFM) measurements performed directly on the microsphere surface reveal a root-mean-square roughness (R_{rms}) of 1.434 nm (Fig. 2b). This value compares favorably to laser and flame-formed microspheres, confirming the high quality and precision of this method[35] and indicates the potential for low surface scattering losses.

The optical cavity Q was measured by coupling light from a tunable laser into and out of the cavity using a tapered optical fiber and scanning the laser across the resonant wavelength. Figure 2c presents the transmission spectrum of a 295 μm diameter microsphere, which shows a resonant wavelength at 1554.015 nm. The linewidth was fit to a Lorentzian, and the intrinsic quality factor was calculated according to coupled mode theory[30] with the value of 1.08×10^6. Quality factor values of this
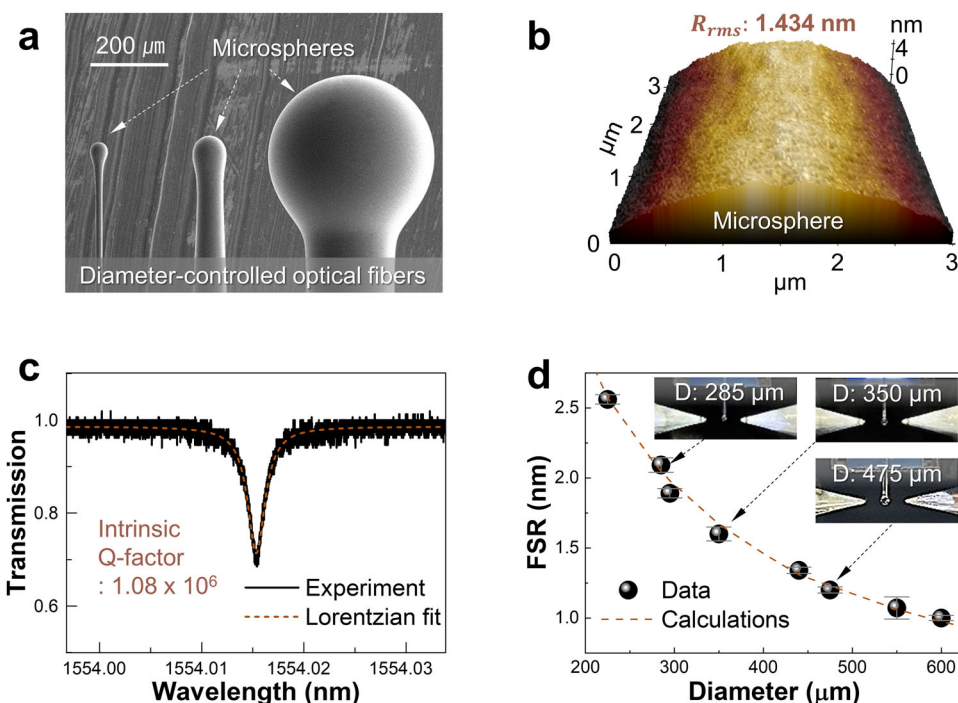
Fig. 2 Characteristics of silica microspheres fabricated by arc fusion method. a SEM image of fabricated microspheres at the ends of diameter-ctontrolled optical fibers. **b** AFM image of fabricated microsphere surface. **c** Measured transmission spectrum of fabricated microsphere on a resonance at 1554.016 nm. **d** Dependence of FSR on the diameter of fabricated microsphere. The error bars represent the standard deviation from the measurement and are smaller than the symbols. Inset: images of fabricated microspheres with different sizes inside the arc fusion setup.

magnitude are sufficient for spectral filtering and for supporting nonlinear optical behaviors.

To further confirm that the devices followed conventional WGM cavity theory, the dependence of the FSR on device diameter was analyzed. This measurement took advantage of the ability to control device geometry using the developed arc fusion method. As shown in Fig. 2d and in accordance with theory outlined in the SI, the FSR is inversely dependent on the diameter. The theoretical prediction is also plotted for reference. The high-Q value of the device confirmed the successful operation of spectral filtering and significant nonlinear interaction between the WGMs and the graphene that is to be synthesized around the resonator.
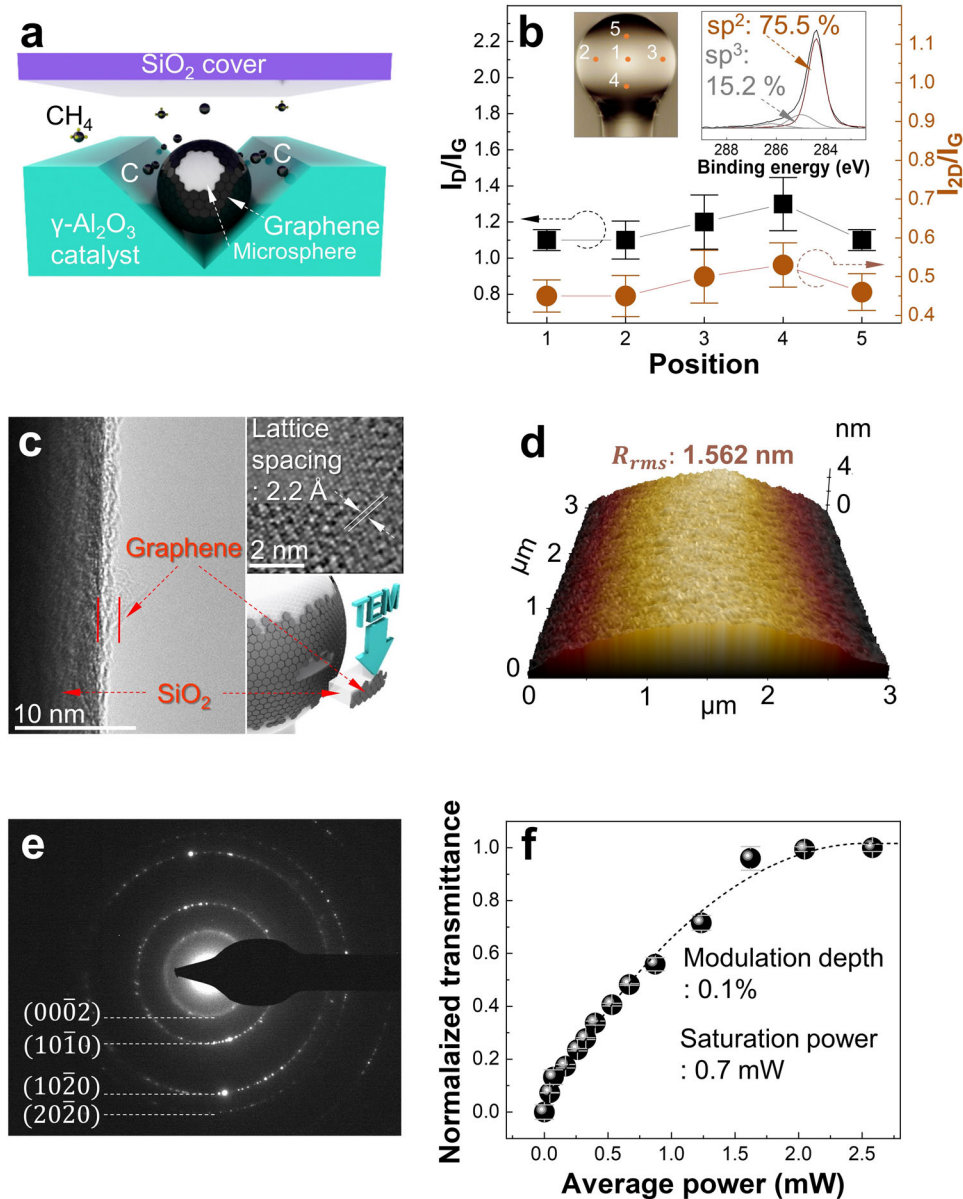
Graphene synthesis and characterization

To maintain a high nonlinear performance, it is critical to achieve a very uniform, contamination-free graphene layer. However, the complex morphology of many integrated photonic devices, including microspheres, is not ideally suited to the most commonly used graphene transfer techniques. The ACS method demonstrated in our prior work overcomes these hurdles[28,29]. Figure 3a shows a schematic illustration of graphene synthesis via the ACS method. Carbon atoms spatially diffuse from the catalyst and provide uniform and direct growth of graphene crystals on the target substrate in an arbitrary 3-dimensional shape without damage and/or imperfections (Supplementary Figs. 4–6). The chemical composition was analyzed using X-ray photoelectron spectroscopy (XPS) and Raman spectroscopy. Because the optical nonlinearity of graphene directly correlates with the concentration of sp^2 hybridized carbon atoms, XPS is a useful tool[36]. The deconvoluted C1s spectrum displayed a dominating peak of 75% of sp^2 bonds at 284.4 eV of binding energy (Fig. 3b inset). This purity is in direct contrast to transferred graphene that shows a high level of contamination[37,38]. To further confirm the

composition, a 532 nm excitation laser is used to probe Raman spectra from different regions of microsphere. The calculated intensity ratios of the D, G, and 2D peaks are presented on Fig. 3b. The ratios of peak intensities I_D/I_G ranged from 1.1 to 1.3, indicating the nearly similar concentration of disorders in graphene around all regions[39]. I_{2D}/I_G intensity ratios ranged from 0.45 to 0.53, indicating the presence of multilayered graphene structure at each inspected area of microsphere[29]. Taken together, the spectroscopic methods indicate a high purity and crystalline graphene layer has been conformally synthesized on the microsphere.

To further confirm the uniformity and crystallinity of the graphene layer, the microcavities and control surfaces are analyzed using high-resolution transmission electron microscopy (HR-TEM), AFM, and selected area electron diffraction (SAED). The HR-TEM data shows that the graphene layer is uniformly deposited at the silica microsphere surface (Fig. 3c). The inset shows the graphene lattice, verifying the 0.22 nm lattice spacing. The surface roughness was measured directly on the microsphere using AFM, and the R_{rms} value is 1.562 nm (Fig. 3d). This value is similar to the un-coated sphere, confirming the high quality and precision of the ACS method. Lastly, SAED is performed. The pattern presented in Fig. 3e shows the randomly stacked graphene crystal planes, revealing polycrystalline nature of synthesized graphene. The estimated d-spacings agree with the previously discussed HR-TEM and Raman studies[40].

To confirm the nonlinear optical performance predicted by the XPS measurements, a balanced twin-detector measurement was performed (Supplementary Fig. 7)[41]. The results which confirm saturable absorption behavior are presented in Fig. 3f. The modulation depth (MD) and saturation power (I_{sat}) were 0.1% and 0.7 mW, indicating that unwanted optical absorption that is induced during the light propagation along the microresonator

Fig. 3 Graphene synthesis and characterization. a Schematic representation of the conformal graphene synthesis process on the microsphere surface with the ACS method. A microsphere was placed between the γ-Al_2O_3 substrate and the silica substrate. Graphene was formed around the resonator surface during the CVD process. **b** Plots of intensity ratios of D, G, 2D peaks, I_D/I_G (black), I_{2D}/I_G (brown) are calculated from the Raman spectra of synthesized graphene. Inset (left): The specific material analysis locations include the equator and both poles. Inset (right): Decomposed C1s spectra of ACS graphene analyzed by XPS. The error bars represent the standard deviation from the measurements and are smaller than the symbols. **c** HR-TEM image of microsphere surface taken at the edge of spherical part of SiO_2 substrate after graphene synthesis. Inset (top): HR-TEM image with a measured lattice spacing of graphene. Inset (bottom): Schematic illustration of TEM imaging procedure. **d** AFM image of microsphere surface after graphene synthesis. **e** SAED pattern with bright dotted rings obtained from the randomly oriented graphene layer stacks. **f** Nonlinear saturable absorption property of ACS graphene measured with balanced twin-detectors. The error bars represent the standard deviation from the measurements and are smaller than the symbols.

interface by graphene was minimized, resulting in a stable mode-locked pulse operation at anomalous dispersion regime[21,42,43].

Operational principles of pulsed laser with high repetition rate

To characterize the ultra-high repetition rate pulsed laser using a single intracavity resonating device with conformal saturable absorber coating, the testing set-up shown in Fig. 4a was used. The optical signal is evanescently coupled from the main laser cavity into the graphene-coated microsphere using a tapered

optical fiber. It propagates around the microsphere and interacts with the graphene layer. The basic principles of pulsed laser generation using a saturable absorber device are shown in Fig. 4b. In the absence of a microcavity, all-optical modes from a CW laser are able to interact with a graphene saturable absorber layer. Using this strategy, the CW laser modes will undergo a conventional passive mode-locking process, resulting in optical pulses with a broad spectral width of high-density phase-locked longitudinal modes[21–23,44]. The repetition rate is inversely proportional to the roundtrip time in the main fiber laser cavity, and it is typically limited to the MHz level, as depicted in Fig. 4c.
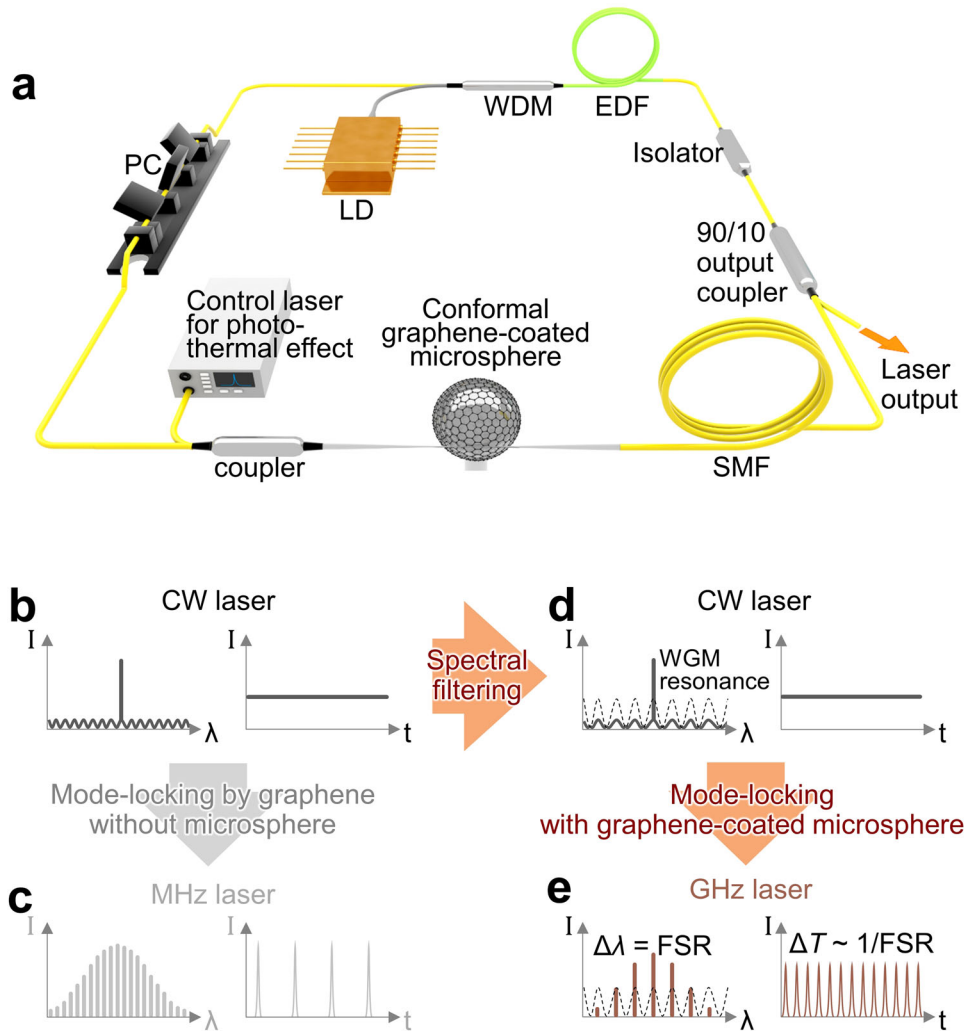
Fig. 4 Experimental setup and operational principles of ultra-high repetition rate laser pulses by directly synthesized graphene-coated microspheres. a Experimental setup for generating ultra-high repetition rate laser pulses based on a fiber ring laser structure that includes a spectral filtering intracavity component combined with optically nonlinear graphene. Note that the control laser was applied to the graphene-coated microsphere in the opposite direction to the circulating pulse laser and was used only for tuning the pulse repetition rate. LD: laser diode, WDM: wavelength-division multiplexer, EDF: Er-doped fiber, SMF: single-mode fiber, PC: polarization controller. **b** Optical spectrum and oscilloscope trace of a CW laser formed in the fiber ring laser main cavity. **c** Optical spectrum and oscilloscope trace of MHz laser pulses mode-locked by graphene without involving the resonant microcavity. The pulse parameters, such as mode spacing, repetition rate, and pulse duration, are determined by the main cavity. **d** Optical spectrum and oscilloscope trace of CW laser that is coupled into the graphene-coated microsphere, in which only the modes spectrally matched with WGM resonance survived. **e** Optical spectrum and pulse train of a GHz laser whose modes were initially filtered by the microsphere and locked in phases with each other by graphene conformally coated around the microsphere. The microsphere properties determine the pulse parameters.

By integrating a microcavity into the system, the CW laser signal is filtered by the resonance of the microcavity, and the filtered WGMs propagate around the microsphere surface, interacting with the graphene layer[24–28]. WGMs that have optical power below the threshold and random phases are suppressed by the absorption of graphene. In contrast, WGMs that phase-lock with each other (i.e., in-phase) form stronger pulses and overcome the graphene absorption. The modes are automatically phase-matched with each other and form ultra-short pulses, as depicted in Fig. 4d. The repetition rate of the generated pulses depends on the FSR of the cavity. As shown in Fig. 2d, the FSR values of the cavities used in the present work range from 1.0 nm to 2.5 nm. Therefore, GHz-rate pulses shown in Fig. 4e are in agreement with the proposed mechanism.

To more quantitatively predict the behavior, the generated mode-locked laser can be theoretically described by a Haus master equation for a fast saturable absorber:

$$\frac{1}{T_r}\frac{\partial}{\partial T}a = (g - l)a + \left(\frac{1}{\Omega_f^2} + jD\right)\frac{\partial^2}{\partial t^2}a + (\gamma - j\delta)|a|^2 a \qquad (1)$$

where T_r is the round-trip time, $a(T,t)$ is the pulse envelope, g is the gain per pass, l is the loss per pass, D is the group velocity dispersion parameter, $\frac{1}{\Omega_f^2}$ and $\frac{\partial^2}{\partial t^2}$ is the filtering action, γ is the self-amplitude modulation coefficient, $\delta = (2\pi/\lambda)n_2 L/A_{eff}$ is the Kerr-coefficient, where λ is the carrier wavelength, n_2 is the nonlinear index, L is the length of medium, and A_{eff} is the effective mode cross-sectional area[44]. Resultant steady state solution can be used to characterize an experimentally generated pulse with its following expression:

$$a(t) = A_0 \text{sech}^{(1+j\beta)}\left(\frac{t}{\tau}\right) \qquad (2)$$
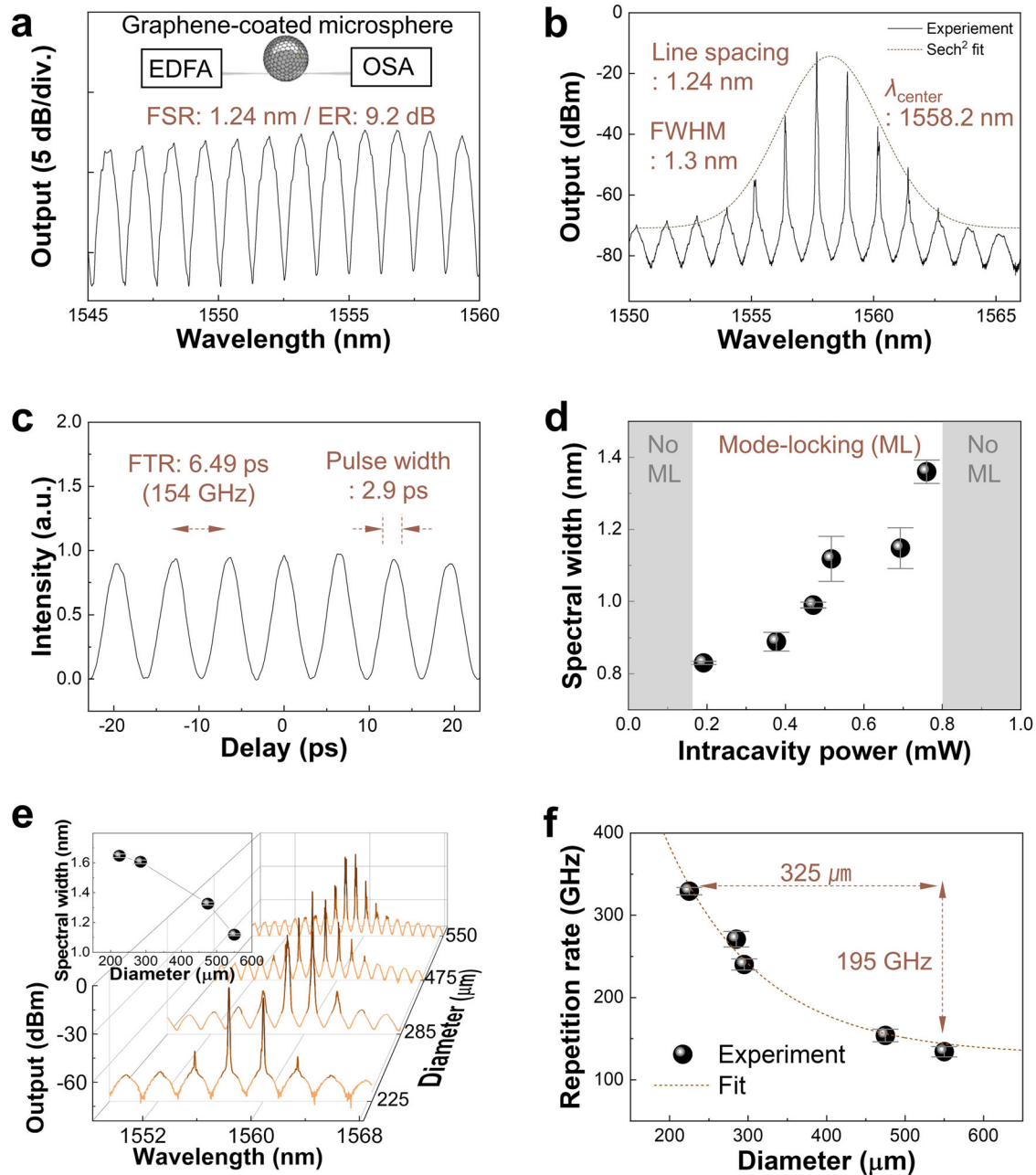
Fig. 5 Characteristics of pulse laser with ultra-high repetition rate. a Optical transmission spectrum of the conformal graphene-coated microsphere with 475 μm diameter. An output from broadband source, EDFA, was coupled into a microsphere through the tapered fiber. The resonance characteristics were detected by an OSA. **b** Optical spectrum of the GHz mode-locked pulses formed by 475 μm graphene-coated microsphere. **c** Measured autocorrelation trace of mode-locked pulses with 2.9 ps duration and 154 GHz repetition rate formed by 475 μm graphene-coated microsphere. **d** Pulse 3 dB spectral width evolution concerning intracavity power in different laser operating regimes. The error bars represent the standard deviation from the measurements and are smaller than the symbols. **e** Pulse optical spectra with respect to the diameter of microsphere. Inset: visualization of the relationship between microsphere diameter and spectral width. The error bars represent the standard deviation from the measurements and are smaller than the symbols. **f** Resultant pulse repetition rates concerning the diameter of microsphere. The error bars represent the standard deviation from the measurements and are smaller than the symbols.

where A_0 is the pulse intensity, β is the propagation constant and τ is the pulse duration[44]. Consequently, the mode-locked laser repetition rate can be dramatically elevated by spectral filtering, which can be explained by the Fourier transformation. Moreover, we can expect higher operating efficiency of the spectral filtering device when it is combined with a nonlinear saturable absorption nanomaterial such as graphene.

Characteristics of pulsed laser with ultra-high repetition rate

The basic optical characterization results of a graphene-coated microsphere with 475 μm diameter are presented in Fig. 5a. The measured FSR and extinction ratio (ER) were 1.24 nm of 9.2 dB, accordingly. All subsequent measurements in Fig. 5 were performed using this device. Figure 5b shows the optical spectrum of the pulsed laser with sech^2 fitting that supports the proposed

passive mode-locking formation mechanism enabled by the graphene-coated microcavity. The central wavelength and 3 dB spectral bandwidth of sech^2 fit envelope output were 1558.2 nm and 1.3 nm, respectively. It is critical to have a high-Q microsphere and a loss-minimized graphene coating to generate a wider spectral envelope, thereby guaranteeing a larger number of filtered modes for a shorter duration of each pulse. The measured line spacing in the optical spectrum was 1.24 nm, which matches the FSR of the microcavity.

Figure 5c presents the pulse train of the GHz pulsed laser measured by autocorrelator. Recorded pulse duration was 2.9 ps, and the free temporal range (FTR) was 6.49 ps which corresponds to 154 GHz repetition rate. The calculated time-bandwidth product (TBP) of generated pulse was 0.318, corresponding to a high-quality bandwidth-limited sech^2-shape pulse. Figure 5d presents the power range of the successful mode-locking operation of the fiber laser. Stable pulses were formed at intracavity powers ranging from 0.19 to 0.76 mW, indicating a correct balance between nonlinearity and chromatic dispersion in the laser cavity. Pulse spectral width growth was recorded from 0.9 nm to 1.3 nm with intracavity power increase. Such pulse behavior can be attributed to the number of modes that survive after coupling with the microsphere and interacting with graphene. A higher density of filtered WGMs forms a broader sech^2 envelope of the pulses at higher intracavity power. On the other hand, at intracavity powers below 0.19 mW and over 0.76 mW, pulse mode-locking was not achievable due to the imbalance between nonlinearity and chromatic dispersion.

Figure 5e presents optical spectra of generated GHz pulsed lasers concerning graphene-coated microspheres with different diameters, as shown in Fig. 2d. A microsphere with 550 μm diameter filtered out the coupled WGMs around the microsphere, resulting in a 1 nm mode spacing corresponding to its FSR. On the other hand, a microsphere with 225 μm diameter filtered out the larger density of intracavity WGMs, maintaining only a few with high intensities, resulting in GHz pulses with spectral distance of 2.64 nm. The inset illustrates the decreasing trend of the pulse spectral width as the diameter of the microsphere increases due to the accumulating absorption loss by graphene layer. Therefore, for GHz pulses generated in a fiber laser with 550 and 225 μm microspheres, the resultant bandwidths of the spectral envelopes were 1.12 and 1.64 nm, respectively. Figure 5f shows changes in pulse repetition rate as related to the diameter of the microspheres. Pulsed lasers formed from graphene-coated microspheres with diameters of 550 and 225 μm showed a repetition rate of 129 and 330 GHz, respectively, demonstrating the ability to control the rate. By adjusting the cavity dimension, a dramatic improvement over conventional mode-locked MHz pulses to GHz mode-locked pulses are achieved, overcoming 4 order of magnitude gap of the repetition rate of main cavity, which was estimated about 13.6 MHz.

Optical tuning of pulse repetition rate

The repetition rate depends on the resonant wavelength and the FSR. Here, all-optical tuning of the repetition rate by leveraging the photo-thermal effect of graphene is demonstrated. The effect is caused by the interaction of the optical field with the device. Because the thermally-induced shift is governed by the dn/dT of the material, the effect becomes more pronounced as the circulating power increases. Due to the positive dn/dT of silica, this thermal change results in an increase in resonant wavelength or decrease in FSR.

In the case of the hybrid graphene-silica devices, this resonant wavelength red-shift is further enhanced by light absorption by the graphene layer (Supplementary Fig. 9). However, as a conductor, the mechanism is different. The energy of carriers excited by light absorption is coupled to optical phonons, and the interaction between carriers and lattice vibration generates heat[45,46] (Fig. 6a).
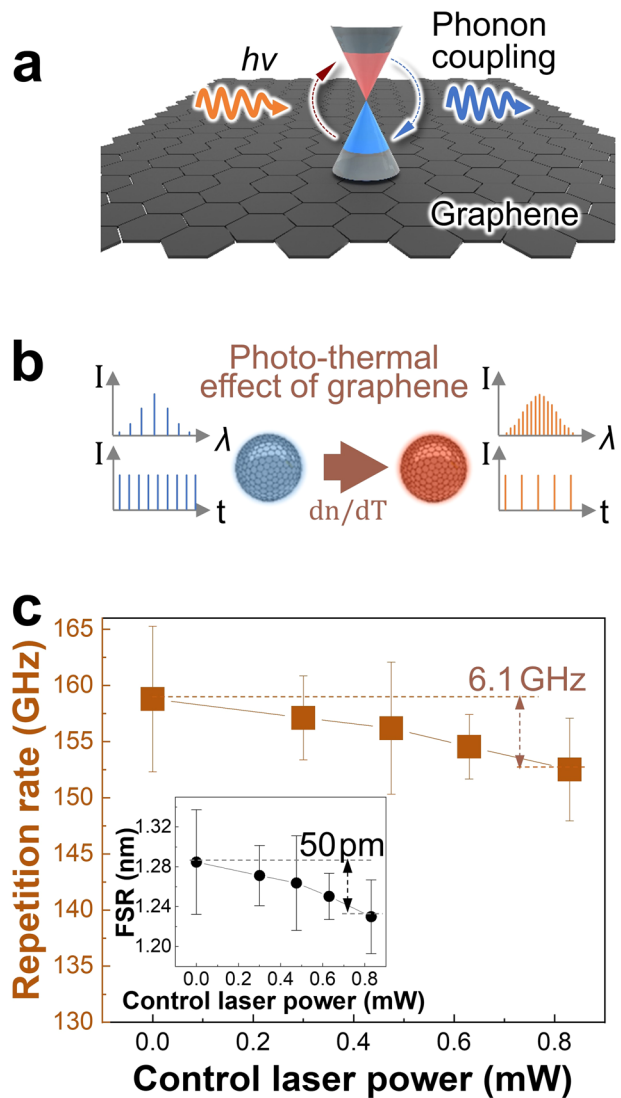
Fig. 6 **Tuning of pulse repetition rate based on the photo-thermal effect of graphene. a** Photo-thermal effect of graphene. **b** Operational principle of repetition rate tuning. **c** Measured pulse repetition rate (brown) and calculated FSR (black) as a function of control laser power. The error bars represent the standard deviation from the measurements and are smaller than the symbols.

The following equation can define the generated heat:

$$q = \frac{1}{2}\varepsilon_0\omega\text{Im}(\varepsilon_r)|\mathbf{E}|^2 \qquad (3)$$

where q is generated heat from graphene, ε_0 is permittivity of vacuum, ω is angular frequency of light, ε_r is relative permittivity of graphene and **E** is electric field in graphene film[47]. Therefore, similar to the case of silica, by increasing the circulating intensity, the resonant wavelength will increase[48].

To confirm all-optical control of the repetition rate, an additional control laser was integrated into the characterization set-up (Fig. 4a). This laser was used to systematically increase the coupled power into the cavity, controlling the cavity's temperature and FSR (Fig. 6b). As can be observed in Fig. 6c, as the input power increased from 0 to 0.8 mW, the repetition rate and the FSR decreased by 6.1 GHz and 50 pm, respectively. Therefore, using a single cavity, the repetition rate can be easily and precisely tuned post-fabrication. This ability provides a materials-driven approach to relaxing fabrication tolerances in ultra-high repetition rate pulse generators.

To summarize, a tunable GHz repetition rate mode-locked laser was designed and demonstrated using a graphene-coated high-Q resonant cavity as an intracavity component for WGM operation. To maintain the requisite optical device and materials performance, an alternative strategy for synthesizing conformal, uniform crystalline layers of graphene directly on the photonic device surfaces was developed, and the chemical, structural, and optical properties were characterized. With minimal degradation in optical loss or nonlinear optical behavior, effective mode filtering by the optical cavity and strong light-matter interaction with the graphene layer was possible. By varying the microcavity diameter during the arc fusion fabrication process, it was possible to modify the GHz frequency. Additionally, the GHz repetition rate can be dynamically tuned in real-time using the photo-thermal effect. This all-optical method provides a unique post-processing approach for tuning the repetition rate within a narrow frequency bandwidth. This type of GHz repetition rate pulse generator has applications in communications, frequency comb management and bio-imaging[49,50]. Moreover, the demonstrated ability to directly synthesize high quality graphene on optical devices with minimal performance degradation has potential impact across numerous fields of science and engineering including quantum studies, sensing, and imaging.

METHODS

Fabrication of microsphere

The silica microsphere was fabricated using the arc fusion method. The coating from a 2 cm piece of optical fiber was removed and cleaned with ethanol. Thereafter, the fiber was cleaved. The fiber end was vertically fixed between two electrodes in a modified arc fusion splicer (TLC-100). After the alignment procedure, an electrical arc (600 mW, 30 s) was applied to the optical fiber end. The final microsphere diameter is determined by controlling the number of arc pulses.

Growth of conformal graphene

Graphene was grown directly onto the nonplanar surface of the silica microsphere in chemical vapor deposition (CVD) furnace. The catalyst used was γ-Al_2O_3 and CH_4 gas (99.995% purity) was used as the carbon source. At the start of the process, the tube was purged with Ar gas for 10 min at a flow rate of 1000 standard cm^3/min (SCCM). The furnace temperature was then increased to 1080 °C under continuous Ar flow. After the target temperature level is reached, CH_4 gas with a flow rate of 35 SCCM was injected into the quartz tube for 40 min. At the end, the CVD furnace was slowly returned to room temperature (30 min) under the CH_4 and H_2.

AFM analysis

The AFM surface topography images were obtained on the High Accuracy Small Sample Scanning Probe Microscope (SPM) XE-100. A Non-Contact Cantilever PPP-NCHR 10 M was used for non-contact measurement mode.

SEM and TEM analysis

SEM images were taken on Teneo VS scanning electron microscope at 10 kV accelerating voltage and 6 nm spot size. TEM images were obtained with a transmission electron microscope TitanTM 80–300 at 300 kV accelerating voltage, 0.1 nm image resolution, and 0.09 nm electron probe size.

Raman spectroscopy

Synthesized graphene was characterized by Raman spectroscopy using high-resolution Renishaw inVia confocal Raman microscope. A 50x microscope objective lens was used to focus 532 nm laser light with a beam size of 2 μm at 2 mW power.

XPS analysis

Synthesized graphene was characterized by X-ray photoelectron spectroscopy using Thermo Scientific Nexsa Spectrometer with microfocus monochromatic X-ray source Al-Kα (1488.6 eV), on_Dual Neutralizer (Ar ion + electrons), and 100 ×100 μm beam spot size.

Laser cavity

An overview of the experimental measurement system is shown in Fig. 4. The laser cavity was created by an erbium-doped fiber amplifier (EDFA) driven by a 980 nm laser diode (LD), wavelength division multiplexer (WDM) and 3 m erbium-doped fiber (EDF) in order to produce 1550 nm light. An optical isolator was embedded into this system in order to provide unidirectional laser operation. This approach avoids optical damage to the equipment, which can be caused by the backward reflections and scattering of the light off of components. A 10 m single-mode fiber (SMF) was inserted to compensate for nonlinearity and group velocity dispersion (GVD) in the laser cavity. A polarization controller (PC) served to adjust the polarization states at each round trip. An output coupler with a 90:10 coupling ratio was used to extract the generated pulse outputs. The photo-thermal effect was studied by integrating an additional control laser into the system. Light from this laser was coupled into the cavity using a tapered optical fiber waveguide, providing repetition rate tuning based on the photo-thermal effect of graphene. A calculated net GVD of the cavity was -0.221 ps^2. The laser output was monitored with an optical spectrum analyzer (Yokogawa AW6370C) and an autocorrelator (HAC-200).

Reporting summary

Further information on research design is available in the Nature Research Reporting Summary linked to this article.

DATA AVAILABILITY

The data that support the findings of this study are available upon reasonable request from the corresponding author. The data are not publicly available due to privacy or ethical restrictions.

REFERENCES

1. Divit, S., Zhu, W., Zhang, C., Lezec, H. & Agrawal, A. Ultrafast optical pulse shaping using dielectric metasurfaces. *Science* **364**, 890–894 (2019).
2. Hafez, H. A. et al. Extremely efficient terahertz high-harmonic generation in graphene by hot Dirac fermions. *Nature* **561**, 507–511 (2018).
3. Sakakura, M., Lei, Y., Wang, L., Yu, Y. & Kazansky, P. G. Ultralow-loss geometric phase and polarization shaping by ultrafast laser writing in silica glass. *Light.: Sci. Appl.* **9**, 15 (2020).
4. Papadopoulos, A. et al. E. Biomimetic omnidirectional antireflective glass via direct ultrafast laser nanostructuring. *Adv. Mater.* **31**, 1901123 (2019).
5. Xiang, C. et al. Laser soliton microcombs heterogeneously integrated on silicon. *Science* **373**, 99–103 (2021).
6. Kim, J. Chip-scale power booster for light. *Science* **376**, 1269 (2022).
7. Stern, B., Ji, X., Okawachi, Y., Gaeta, A. L. & Lipson, M. Battery-operated integrated frequency comb generator. *Nature* **562**, 401–40502 (2018).
8. Cheng, H. et al. High-repetition-rate ultrafast fiber lasers. *Opt. Express* **26**, 16411–16421 (2018).
9. Bogusławski, Y. et al. Graphene actively mode-locked lasers. *Adv. Funct. Mater.* **28**, 1801539 (2018).
10. Abas, A. F. et al. Dispersion management and pulse characterization of graphene-based soliton mode-locked lasers. *Appl. Sci.* **12**, 3288 (2022).
11. Rosenblum, S., Lovsky, Y., Arazi, L., Volmer, F. & Dayan, B. Cavity ring-up spectroscopy for ultrafast sensing with optical microresonators. *Nat. Commun.* **6**, 6788 (2015).
12. Riemensberger, J. et al. Massively parallel coherent laser ranging using a soliton microcomb. *Nature* **581**, 164–170 (2020).

13. Stassen, E. et al. Ultra-low power all-optical wavelength conversion of high-speed data signals in high-confinement AlGaAs-on-insulator microresonators. *APL Photon* **4**, 100804 (2019).

14. Newman, Z. L. et al. Architecture for the photonic integration of an optical atomic clock. *Optica* **6**, 680–685 (2019).

15. Martinez, A. & Yamashita, S. 10 GHz fundamental mode fiber laser using a graphene saturable absorber. *Appl. Phys. Lett.* **101**, 041118 (2012).

16. Kwon, D., Jeong, D., Jeon, I., Lee, H. & Kim, J. Ultrastable microwave and soliton-pulse generation from fibre-photonic-stabilized microcombs. *Nat. Commun.* **13**, 381 (2022).

17. Wang, W. et al. Repetition rate multiplication pulsed laser source based on a microring resonator. *ACS Photon* **4**, 1677–1683 (2017).

18. Debnath, P. C. & Yeom, D.-I. Ultrafast fiber lasers with low-dimensional saturable absorbers: status and prospects. *Sensors* **21**, 3676 (2021).

19. Autere, A. et al. Nonlinear optics with 2D layered materials. *Adv. Mater.* **30**, 1705963 (2018).

20. Castro Neto, A. H., Guinea, F., Peres, N. M. R., Novoselov, K. S. & Geim, A. K. The electronic properties of graphene. *Rev. Mod. Phys.* **81**, 109–162 (2009).

21. Ryu, B., Kim, J. T. & Song, Y. W. Graphene-dispersed polymer waveguide for efficient formation of mode-locked lasers at extremely low graphene concentration. *Carbon* **166**, 123–130 (2020).

22. Kovalchuk, O., Uddin, S., Lee, S. & Song, Y. W. Graphene capacitor-based electrical switching of mode-locking in all-fiberized femtosecond lasers. *ACS Appl. Mater. Interfaces* **12**, 54005–54011 (2020).

23. Lee, E. J. et al. Active control of all-fibre graphene devices with electrical gating. *Nat. Commun.* **6**, 6851 (2015).

24. Liu, M., Tang, R., Luo, A.-P., Xu, W.-C. & Luo, Z.-C. Graphene-decorated microfiber knot as a broadband resonator for ultrahigh-repetition-rate pulse fiber lasers. *Photonics Res.* **6**, C1–C7 (2018).

25. Suzuki, T. S. L. P. et al. Design of a passively mode-locking whispering-gallery-mode microlaser. *J. Opt. Soc. Am. B* **38**, 3172–3178 (2021).

26. Lee, S. & Song, Y. W. Graphene self-phase-lockers formed around a Cu wire hub for ring resonators incorporated into 57.8 gigahertz fiber pulsed lasers. *ACS Nano* **14**, 15944–15952 (2020).

27. Ding, Z., Chen, Y. & Xu, F. Multifunctional all-fiber mode-locked laser based on graphene-integrated polarization-dependent microfiber resonator. *Opt. Laser Technol.* **143**, 107381 (2021).

28. Uddin, S., Kim, S., Choi, J. & Song, Y. W. Conformal graphene directly synthesized on a femtosecond laser-scribed in-fiber microstructure for high-energy ultrafast optical pulses. *ACS Nano* **15**, 20300–20310 (2021).

29. Uddin, S. & Song, Y. W. Atomic carbon spraying: direct growth of graphene on customized 3D surfaces of ultrafast optical devices. *Adv. Opt. Mater.* **8**, 1902091 (2020).

30. Cai, L., Pan, J. & Hu, S. Overview of the coupling methods used in whispering gallery mode resonator systems for sensing. *Opt. Lasers Eng.* **127**, 105968 (2020).

31. Bao, Q. et al. Atomic layer graphene as saturable absorber for ultrafast pulsed laser. *Adv. Funct. Mater.* **19**, 3077–3083 (2009).

32. Armani, A. M., Kulkarni, R. P., Fraser, S. E., Flagan, R. C. & Vahala, K. J. Label-free, single-molecule detection with optical microcavities. *Science* **317**, 783–787 (2007).

33. Wu, L. et al. Greater than one billion Q factor for on-chip microresonators. *Opt. Lett.* **45**, 5129–5131 (2020).

34. He, J. et al. All-optical reversible control of integrated resonant cavity by a self-assembled azobenzene monolayer. *Opt. Express* **28**, 22462–22477 (2020).

35. Vernooy, D. W., Ilchenko, V. S., Mabuchi, H., Streed, E. W. & Kimble, H. J. High-Q measurements of fused-silica microspheres in the near infrared. *Opt. Lett.* **23**, 247–249 (1998).

36. Karankova, S. et al. Optical saturable absorption of conformal graphene directly synthesized on nonlinear device surfaces. *Appl. Surf. Sci.* **611**, 155641 (2023).

37. Wang, M. et al. Single-crystal, large-area, fold-free monolayer graphene. *Nature* **596**, 519 (2021).

38. Wang, F. et al. Wideband-tuneable, nanotube mode-locked, fibre laser. *Nat. Nanotech* **3**, 738–742 (2008).

39. Lucchese, M. M. et al. Quantifying ion-induced defects and Raman relaxation length in graphene. *Carbon* **48**, 1592–1597 (2010).

40. Limbu, T. B. et al. A novel approach to the layer-number-controlled and grain-size- controlled growth of high quality graphene for nanoelectronics. *ACS Appl. Nano Mater.* **1**, 1502–1512 (2018).

41. Ahmad, H., Yusoff, N., Monajemi, H. & Reduan, S. A. Nickel phosphate as a C-band optical pulse modulator. *Appl. Phys. B* **125**, 132 (2019).

42. Zhang, F., Han, S., Liu, S. Y., Wang, Z. P. & Xu, X. G. Dependence of the saturable absorption of graphene upon excitation photon energy. *Appl. Phys. Lett.* **106**, 091102 (2015).

43. Chu, S. et al. Ultrafast saturable absorption devices incorporating efficiently electrosprayed carbon nanotubes. *Appl. Phys. Lett.* **96**, 051111 (2010).

44. Haus, H. A. Mode-locking of lasers. *IEEE J. Sel. Top. Quantum Electron.* **6**, 1173–1185 (2000).

45. Lee, S., Kim, J. T. & Song, Y. W. Graphene-incorporated soft capacitors for mechanically adjustable electro-optic modulators. *ACS Appl. Mater. Interfaces* **10**, 40781–40788 (2018).

46. Massicotte, M., Soavi, G., Principi, A. & Tielrooij, K.-J. Hot carriers in graphene – fundamentals and applications. *Nanoscale* **13**, 8376–5411 (2021).

47. Gan, X. et al. Graphene-assisted all-fiber phase shifter and switching. *Optica* **2**, 468–471 (2015).

48. Soltani, S. & Armani, A. M. Optothermal transport behavior in whispering gallery mode optical cavities. *Appl. Phys. Lett.* **105**, 051111 (2014).

49. Miakami, H. et al. Ultrafast confocal fluorescence microscopy beyond the fluorescence lifetime limit. *Optica* **5**, 117–126 (2018).

50. Hillerkuss, D. et al. 26 Tbit s^{-1} line-rate super-channel transmission utilizing all-optical fast Fourier transform processing. *Nat. Photon.* **5**, 364–371 (2011).

ACKNOWLEDGEMENTS

AUTHOR CONTRIBUTIONS

O.K., S.L., and Y.W.S. conceived the idea and designed the experiments. O.K., and S.L. fabricated the samples, performed the experiments, and analyzed the data. O.K., S.L., H.M., A.M.A., and Y.W.S. provided in-depth discussion of the project. O.K., S.L., A.M.A., and Y.W.S. wrote the manuscript. O.K. and S.L. contributed equally to this work. All authors have given approval for the final version of the manuscript.

COMPETING INTERESTS

A. M. A. is Sr. Director of Physical Sciences and Engineering at the Ellison Institute of Technology (paid position).

ADDITIONAL INFORMATION

Supplementary information The online version contains supplementary material available at https://doi.org/10.1038/s41699-024-00440-5.

Correspondence and requests for materials should be addressed to Andrea M. Armani or Yong-Won Song.

Reprints and permission information is available at http://www.nature.com/reprints

Publisher's note Springer Nature remains neutral with regard to jurisdictional claims in published maps and institutional affiliations.